Title: Rate of photosynthetic acclimation to fluctuating light varies widely among genotypes of wheat

Running title: Variation in photosynthetic acclimation kinetics in wheat

William T. Salter[1] (william.salter@sydney.edu.au)
Andrew M. Merchant[1] (andrew.merchant@sydney.edu.au)
Richard A. Richards[2] (richard.richards@csiro.au)
Richard Trethowan[1] (richard.trethowan@sydney.edu.au)
Thomas N. Buckley[3,*] (tnbuckley@ucdavis.edu)

[1] School of Life and Environmental Sciences, Sydney Institute of Agriculture, The University of Sydney, Brownlow Hill, NSW 2570, Australia
[2] CSIRO, Agriculture and Food, GPO Box 1700, Canberra, ACT, 2601, Australia
[3] Department of Plant Sciences, University of California, Davis, Davis, CA 95616, USA

*Corresponding author: +1 916 917 9217

Submission date: 5th October 2018
Number of tables: 0
Number of figures: 7 (2 black and white, 5 in colour for print and online)
Word count: 5214

Highlight

Significant variation exists in the acclimation time of photosynthesis following dark-to-light transitions across wheat genotypes, under field and controlled conditions. Slow acclimation reduced daily carbon assimilation by up to 16%.

Abstract

Crop photosynthesis and yield are limited by slow photosynthetic induction in sunflecks. We quantified variation in induction kinetics across diverse genotypes of wheat for the first time. In a preliminary study using penultimate leaves of 58 genotypes grown in the field, we measured induction kinetics for maximum assimilation rate (A_{max}) after a shift from full darkness to saturating light (1700 μmol m^{-2} s^{-1}) with 1-4 replicates per genotype. We then grew 10 of these genotypes with contrasting responses in a controlled environment and quantified induction kinetics of carboxylation capacity (V_{cmax}) from dynamic A vs c_i curves after a shift from low to high light (50 to 1500 μmol m^{-2} s^{-1}), with 5 replicates per genotype. Within-genotype median time for 95% induction (t_{95}) varied from 8.4 to 23.7 min across genotypes for A_{max} in field-grown penultimate leaves, and from 6.7 to 10.4 min for V_{cmax} in chamber-grown flag leaves. Our simulations suggested that non-instantaneous acclimation reduces daily net carbon gain by up to 16%, and that breeding to speed up V_{cmax} induction in the slowest genotype to match that in the fastest genotype could increase daily net carbon gain by more than 4%, particularly for leaves that experience predominantly short-duration sunflecks.

Keywords: photosynthesis, wheat, rubisco activase, sunfleck, phenotyping, modelling.

Introduction

Global food security is threatened by growing populations and diminishing increases in crop yield potential. To ensure future food security, improvements need to be made to plant yield traits that have previously been overlooked in crop breeding programs, such as dynamic properties of photosynthesis. The efficiency of photosynthetic machinery under fluctuating environmental conditions has been identified as a key target for improvement (Taylor & Long, 2017; Murchie *et al.*, 2018). In particular, the light environment of crop canopies is highly dynamic, with fluctuations occurring on the scale of seconds to minutes (Slattery *et al.*, 2018). On clear days, leaves at the top of the canopy are generally exposed to direct sunlight for the majority of the day, whilst leaves in the lower canopy rely on light in the form of sunflecks. These sunflecks can account for up to 90% of the daily available light (Pearcy, 1990).

The impact of rapid shifts in photosynthetic photon flux density (PPFD) on carbon balance is influenced by a number of physiological factors. Diffusion of CO_2 through stomata and the mesophyll (controlled by conductances g_s and g_m respectively) can limit induction of photosynthesis (Lawson & Vialet-Chabrand, 2018), and conversely, slow deactivation of energy-consuming photoprotective mechanisms when leaves enter shadeflecks can reduce net carbon gain (Kromdijk *et al.*, 2016). Slow acclimation of photosynthesis following shade to sun transitions can also substantially reduce carbon assimilation in crop canopies. Activation of ribulose-1,5-bisphosphate carboxylase/oxygenase (Rubisco) is considered to be a critical constraint on photosynthetic induction to shade-sun transitions (Soleh *et al.*, 2016; Taylor & Long, 2017; Morales *et al.*, 2018). In a recent study, Taylor & Long (2017) predicted that carbon assimilation could be inhibited by up to 21% in wheat (*Triticum aestivum*) by slow induction of Rubisco in response to fluctuating light conditions. If this inefficiency could be reduced, whole canopy carbon assimilation would be improved, potentially leading to increases in yield (Long et al. 2006).

Screening for genetic variation in photosynthetic activation time would increase our fundamental understanding of this process and patterns in variation and dynamics of the response would allow us to identify whether this trait is a valid target for improvement through conventional breeding. However, although some variation in the kinetics of

81 photosynthetic acclimation has been identified across soybean genotypes (Soleh *et al.*,
82 2016; Soleh *et al*. 2017), there is little information available regarding the diversity of this
83 trait in wheat. Taylor and Long (2017) examined only a single genotype, partly due to the
84 arduous nature of the "dynamic *A* vs c_i" method they used to characterize the kinetics of
85 Rubisco activation *in vivo*. Other less direct methods such as *in vitro* Rubisco assays, or high-
86 throughput phenotyping (HTP) field techniques such as multispectral imaging, could be
87 applied more readily to the task of phenotyping many genotypes. However, *in vitro* assays
88 do not capture the interaction of diffusional and biochemical induction. Stomatal and
89 mesophyll diffusion influence [CO_2] in chloroplasts, which in turn regulates Rubisco activase
90 (Portis *et al.*, 1986) – and HTP methods cannot yet quantify photosynthetic rate *per se*, nor
91 its induction kinetics. Direct measurement of gas exchange in intact leaves thus remains, in
92 our view, the only suitable method for phenotyping these traits.
93
94 We used a three-phase approach to quantify the extent of genetic variation in
95 photosynthetic acclimation kinetics in wheat and the potential for directed breeding to
96 enhance productivity by harnessing this variation. First, we measured the kinetics of
97 acclimation for CO_2-saturated photosynthesis after a shift from darkness to saturating light
98 in penultimate leaves of 58 genotypes of field-grown wheat. Second, we then studied
99 acclimation kinetics more intensively for a subset of 10 of these genotypes, using the
100 dynamic *A* vs c_i method to quantify induction of RuBP carboxylation and regeneration
101 capacities over time after a switch from low to high light. Finally, we used modeling to
102 quantify the improvement in diurnal net carbon gain that could be achieved by breeding for
103 faster photosynthetic induction within the observed range of variation across genotypes.
104
105

Methods

Plant material

Detailed analysis of photosynthetic acclimation was conducted on wheat grown under controlled conditions in June/July 2018. 10 genotypes were selected from those grown in the field the previous year (Table S1). Seed was sown in 5 l pots with compost mix containing a slow release fertiliser (Evergreen Garden Care Australia, Bella Vista, NSW, Australia). Day and night temperatures were maintained at 23.7 ± 1.7°C and 12.0 ± 1.8°C (mean ± s.d.) respectively, and relative humidity at 67.2 ± 6.1% and 74.0 ± 8.1%. Growth CO_2 concentration was 482.2 ± 23.2 µmol mol^{-1} across the course of the experiment. Light was supplied by LED growth lamps (LX602C; Heliospectra AB, Göteborg, Sweden) and provided a PPFD of 800 µmol m^{-2} s^{-1} at the leaf surface. Seedlings were thinned to one per pot after germination. Plants were watered twice daily to field capacity. All gas exchange measurements were taken on the mid-section of a fully expanded flag leaf during heading or anthesis (the distribution of Zadoks phenological growth stages during these measurements is shown in Figure S1).

For measurement of photosynthetic acclimation in field-grown plants, wheat was planted in 2 x 6 m plots with 5 sowing rows per plot in Narrabri, NSW, Australia in late May 2017. 58 genotypes were examined here (Table S1). Measurements were made on 03-18 Sep 2017, within two weeks before or after anthesis (the distribution of Zadoks phenological stages across the field measurement campaign is shown in Figure S1).

Detailed analysis of acclimation to light in flag leaves of wheat grown in a controlled environment

Plants were moved from the controlled environment room to a temperature stable laboratory at 25°C. Photosynthetic light response curves were recorded using a LI-6400 gas exchange system (Li-Cor, Lincoln, NE, USA) on one plant of each genotype. Leaves were equilibrated to chamber conditions (leaf temperature 25°C; leaf vapour pressure deficit 1.0-1.5 kPa; cuvette CO_2 (c_a) 400 µmol mol^{-1}; and PPFD 1500 µmol m^{-2} s^{-1} provided by LEDs in the chamber head) for at least 40 min to allow them to reach steady state. PPFD was then reduced through 1200, 1000, 800, 600, 500, 400, 300, 200, 150, 100, 50 and 0 µmol m^{-2} s^{-1}, with measurements taken immediately after chamber conditions had stabilized at each

level. Light responses curves were fitted to a non-rectangular hyperbola model using nonlinear least squares in R (*nls*; R Language and Environment); i.e., the lesser root *A* of

$$\theta\left(A-R_d\right)^2-\left(\phi i+A_{sat}\right)\left(A-R_d\right)+\phi iA_{sat}=0 \quad (1)$$

where i is PPFD, A_{sat} is the asymptotic limit of A at high PPFD, θ is a dimensionless parameter < 1 , ϕ is the initial slope of A_{eq} vs i, and R_d is day respiration rate. A_{sat}, θ, ϕ and R_d were fitted empirically.

Dynamic *A vs* c_i responses were recorded using four Walz GFS-3000 gas exchange systems (Heinz Walz GmbH, Effeltrich, Germany), using the method of Taylor & Long (2017). The acclimation of photosynthesis following transition from shade to saturating light was measured at a number of different c_a values, and composite *A vs* c_i curves were generated for each relative time point during induction. Leaf temperature was held at 25°C and VPD_{leaf} at 1.0 kPa. Each leaf was first brought to a steady state at c_a 400 µmol mol^{-1} and PPFD 1500 µmol m^{-2} s^{-1} (found to be saturating in our light response curves) over 40 min, and PPFD in the leaf chamber was then dropped to 50 µmol m^{-2} s^{-1} for 30 min. During this 'dark phase' the c_a was also reduced to 100 µmol mol^{-1} to inhibit stomatal closure, as per guidelines in Taylor & Long (2017). Prior to induction the c_a was increased to the desired value for induction. Induction of photosynthesis was initiated with a step change to PPFD 1500 µmol m^{-2} s^{-1}, and measurements recorded every 10 seconds for 15 min. This 30 min dark – 15 min light cycle was repeated at induction c_a of 50, 100, 200, 300, 400, 500, 600, 800 and 1000 µmol mol^{-1}.

A vs c_i curves were generated for each 10 s time point after induction of photosynthesis. The Farquhar et al. (1980) photosynthesis model was fitted to these curves using the 'plantecophys' package in R (bilinear fitting method; Duursma, 2015) to provide estimates of Rubisco carboxylation capacity (V_{cmax}) and electron transport rate (J). R_d was set at 1.9 µmol m^{-2} s^{-1} and θ was set at 0.67 (from our light response curves). We also provided the Michaelis-Menten coefficient and the photorespiratory compensation point, calculated from the mean leaf temperature as per Bernacchi et al. (2001). Temperature corrections

were performed during the fitting process to provide values of V_{cmax} and J at 25°C. The script used for curve fitting is provided in Supporting Information File S2.

For each leaf, we modeled the observed timecourse of induction of V_{cmax} using a two-phase exponential function of time:

$$V_{\mathrm{cmax}}(t) = V_{mi} + \left(V_{mf} - V_{mi}\right)\left\{ f\left(1 - \exp\left(-\frac{t}{\tau_{fast}}\right)\right) + (1-f)\left(1 - \exp\left(-\frac{t}{\tau_{slow}}\right)\right)\right\} \quad (2)$$

where the parameters (V_{mi} and V_{mf} are the initial and final (fully acclimated) values of V_{cmax}, τ_{fast} and τ_{slow} are time constants for fast and slow phases of acclimation, respectively, and f is a weighting factor between zero and one) were estimated by using Solver in MS Excel to minimize the sum of squared differences between measured and modeled V_{cmax}. We found that this two-phase model produced a substantially better fit to our data than a single-phase model as used by Taylor and Long (2017), with r^2 ranging from 0.957 to 0.996 (median = 0.990).

Photosynthetic acclimation to light in penultimate leaves of field grown wheat

We used OCTOflux to measure photosynthetic acclimation upon transition from darkness to saturating light in penultimate leaves of 58 genotypes of field grown wheat. This system is described elsewhere (Salter et al., 2018). It is an open-flow single-pass differential gas exchange system with eight leaf chambers (5×11 cm), designed to maximize throughput for measurements of CO_2- and light-saturated net photosynthesis rate (A_{max}). Each chamber has a white LED light source above the adaxial leaf surface, a Propafilm window, four small mixing fans and a type T thermocouple kept appressed to the abaxial surface. Stable dry air is created by mixing CO_2 and dry air from pressurized cylinders with mass flow controllers into a buffering volume (~40 L) containing a powerful fan. This gas is then split into nine streams: a reference stream, which flows through the reference cell of a differential infrared gas analyzer (IRGA; Li-7000, Li-Cor, Lincoln, Nebraska), and eight sample streams, each of which runs through a mass flow meter to a leaf chamber and back to the IRGA, where it is

198 either vented to the atmosphere or directed through the IRGA sample cell, using solenoid
199 valves.
200
201 Tillers were cut in the field, immediately recut under distilled water and placed into
202 darkness and transported by vehicle to the laboratory (about 1 km away; time from cutting
203 to laboratory was 5-15 min), and kept in darkness for a further 0 – 30 minutes before
204 measurement. Each leaf was enclosed in a leaf chamber and exposed to saturating PPFD
205 (1700 µmol m^{-2} s^{-1}) and ambient CO_2 (4800 – 5000 µmol mol^{-1}), and then allowed to
206 acclimate to these conditions. To verify that A_{max} measured at these high c_a values did not
207 differ substantially from the true A_{max}, which occurs at the transition point between RuBP-
208 regeneration-limited and triose phosphate utilization (TPU) limited photosynthesis, we
209 measured traditional A vs c_i curves in 18 leaves and extrapolated these to high c_a using a
210 biochemical model (Farquhar et al. 1980) as extended by Busch et al. (2018), and found that
211 A_{max} at 5000 µmol mol^{-1} was an excellent proxy for true A_{max} (r^2 = 0.9841, slope = 0.9968;
212 Figure S2). Full details of these tests are given in Salter et al. (2018).
213
214 The present study took advantage of the fact that the sample gas stream from one of the
215 eight chambers could be continuously measured during photosynthetic acclimation to
216 saturating light. We recorded net CO_2 assimilation rate every two seconds until stability was
217 achieved (average ~14 min), and the record of A vs time was then modeled with the
218 following sigmoidal equation:
219
220 (3) $$A(t) = A_{init} + (A_{max} - A_{init})\exp(-a \cdot \exp(-bt))$$
221
222 where A_{init}, A_{max}, a and b are positive empirical parameters fitted by using Solver (GRG
223 nonlinear engine) in Microsoft Excel to minimize the sum of squared differences between
224 measured and modeled A. The times for A to rise by 25%, 75% and 95% of the difference
225 between A_{init} and A_{max} (t_{25}, t_{75} and t_{95}, respectively) were then calculated from the fitted
226 parameters, as $t_x = \ln(a/\ln(1/[0.01 \cdot x]))/b$, where x = 25, 75 or 95. The "rise time," or the time
227 required for A to increase through the middle 50% of its dynamic range, was calculated as
228 $t_{75} - t_{25}$.

Because the workflow was organized around the broader phenotyping study (in which 160 genotypes were measured), replication was unbalanced among the 58 genotypes for which we recorded acclimation kinetics, with n = 1 to 4 replicate plants per genotype.

Modeling impact of acclimation kinetics on carbon gain

We simulated the impact of observed variability in photosynthetic acclimation kinetics on diurnal carbon gain for different sunfleck lengths and canopy positions, using a modeling approach similar to that of Taylor and Long (2017), and simulating V_{cmax} induction kinetics using median kinetic parameters for the slowest and fastest of the 10 genotypes studied. To assess the role of sunfleck length and canopy position, we calculated irradiance based on expressions given by Retkute et al. (2018) and de Pury and Farquhar (de Pury & Farquhar, 1997), rather than the sample ray tracing model output used by Taylor and Long (2017). The modeling approach is described in detail in Appendix S1; sample diurnal traces of leaf irradiance, including alternating sunflecks and shadeflecks, are shown in Figure 1.

Analysis of A vs c_i data with the 'one-point method'

We tested whether the 'one-point method' of De Kauwe et al. (2016) would provide robust estimates of V_{cmax} during photosynthetic acclimation to dark-to-light transitions. For this analysis we used the dark-to-light photosynthetic induction at c_a 400 µmol mol^{-1} from our dynamic A vs c_i analysis, and estimated V_{cmax} by fitting the Farquhar et al. (1980) model to the data using the 'plantecophys' package in R (Duursma, 2015).

Statistical analysis

We tested for differences among genotypes in functional parameters of acclimation kinetics (t_{95} and t_{75}-t_{25}) using analysis of variance (function aov() in base R) with genotype as a categorical independent variable and t_{95}, etc., as dependent variables (after transformation to improve normality, by inversion [i.e., $y = 1/t_{95}$] for chamber-grown plants, and by log transformation for field-grown plants). Outliers for t_{95} and t_{75}-t_{25} were removed from the V_{cmax} dataset on the basis of a Grubbs test (R package 'outliers') applied to each genotype; this resulted in removal of three values for t_{95} and four for t_{75}-t_{25}.

Results

Measurement and modeling of acclimation kinetics

A vs c_i curves fit to each 10 s interval following transition from shade (50 µmol m^{-2} s^{-1}) to saturating light (1500 µmol m^{-2} s^{-1}) revealed limitations imposed by V_{cmax} at lower c_i and by *J* at higher c_i throughout induction. Whilst specific acclimation times varied between individual leaves and among genotypes (fitted dynamic *A* vs c_i curves for a slow and a fast acclimating leaf are shown in Fig 2a and 2b respectively), general trends in induction kinetics were clear (Fig S3). Both V_{cmax} and *J* increased immediately after transition to saturating light, however *J* increased more rapidly than V_{cmax} in the first three minutes and also saturated more quickly. As a result, $c_{i,trans}$ (the c_i at which the primary limitation imposed on photosynthesis switches between V_{cmax} and *J*) rose to a maximum of 563 ± 3.2 µmol mol^{-1} three minutes after transition to saturating light, decreasing to 422 ± 4.1 µmol mol^{-1} after seven minutes and remaining relatively stable after this time (Fig S3c). The high values of $c_{i,trans}$ throughout induction indicate that V_{cmax} is likely always limiting to photosynthesis under field conditions (assuming c_a of approx. 400 µmol mol^{-1}). A two-phase exponential model was fitted to the measured V_{cmax} data with r^2 ranging from 0.957 to 0.996 (median = 0.990), a representative timecourse of V_{cmax} induction is shown in Figure 3b.

Photosynthetic induction kinetics of plants grown under field conditions differed from those grown under controlled conditions, specifically there was an initial lag phase after transition to saturating light. A representative timecourse of A_{max} induction of field grown plants is shown in Figure 3a. A sigmoidal equation was fitted to the acclimation kinetics of A_{max} of field grown plants with median $r^2 > 0.99$.

Variation in photosynthetic induction kinetics

For A_{max} in penultimate leaves of field-grown wheat, within-genotype median t_{95} (the time for A_{max} to rise through 95% of its dynamic range) ranged from 8.4 to 23.7 min across genotypes (Fig 4a). The within-genotype median for $t_{75} - t_{25}$ (the time required for A_{max} to increase through the middle 50% of its dynamic range) varied from 1.5 to 7.6 min (Fig 4b). Differences among genotypes were not significant for either variable ($F(57,73) = 0.8$, p =

292 0.81 for t_{95}, and $F(57,73) = 0.94$, $p = 0.6$ for $t_{75} - t_{25}$). Across genotypes the final A_{max} was
293 unrelated to t_{95} ($r^2 = 0.027$, $p = 0.058$) or $t_{75} - t_{25}$ ($r^2 < 0.001$, $p = 0.923$) (Fig S4a and S4c).
294
295 The rate of induction also varied greatly across genotypes for V_{cmax} in flag leaves of chamber-
296 grown wheat. Within-genotype medians ranged from 6.7 to 10.4 for t_{95}, and from 2.2 to 3.1
297 for $t_{75} - t_{25}$ (Fig 4c,d). Differences among genotypes were highly significant for t_{95} ($F(9,37) =$
298 3.97, $p = 0.0013$), but not significant for $t_{75} - t_{25}$ ($F(9,37) = 1.99$, $p = 0.07$). The corresponding
299 within-genotype median time constants for the fast and slow phases of acclimation, τ_{fast} and
300 τ_{slow}, respectively, ranged from 0.05 min to 0.51 min (τ_{fast}) and from 2.6 to 4.5 min (τ_{slow});
301 the weighting factor for the fast phase (f) was 0.39 in the fastest genotype and 0.49 in the
302 slowest. Figure 5 shows representative time-courses of acclimation of normalized V_{cmax}
303 corresponding to these lower and upper deciles for τ_{fast} and τ_{slow}. The final V_{cmax} was
304 unrelated to t_{95} ($r^2 = 0.072$, $p = 0.060$) but was loosely correlated with $t_{75} - t_{25}$ ($r^2 = 0.146$, $p =$
305 0.006) (Fig S4b and S4d).
306
307 *Simulated effect of variation in acclimation kinetics on diurnal carbon gain*
308 Our simulations predicted that non-instantaneous acclimation of photosynthesis to
309 sunflecks could reduce daily carbon gain by as much as 16% (Figure 6a). The reduction was
310 generally greatest for shorter-duration sunflecks, because photosynthesis has less
311 opportunity to approach its fully acclimated "target" value during short sunflecks. This
312 reduction was greater for the slowest genotype than for the fastest under most conditions,
313 with the exception of short-duration sunflecks in upper-canopy leaves (LAI = 0.25 m^2 m^{-2})
314 (Figure 6a). Leaf orientation had fairly small effects on simulated carbon losses due to slow
315 induction (Figure S5), so results presented in the main text were integrated over a spherical
316 leaf angle distribution.
317
318 To consider the gains that could realistically be achieved by breeding, given the variability
319 we observed, we also computed the % loss of daily carbon gain using the "fast" acclimating
320 genotypes as the baseline for comparison with "slow" genotypes, rather than using
321 instantaneous acclimation as the baseline (Fig 6b). The relative advantage of faster
322 acclimation was greatest for sunflecks of short to intermediate duration; for example, for 8-

323 min sunflecks, "slow" genotypes gained 2.9 to 4.3% less carbon over a day than "fast"
324 genotypes.
325
326 **Discussion**
327 We found greater than two-fold variation across genotypes of wheat in the time required
328 for 95% photosynthetic induction (t_{95}) after exposure to saturating light, both for maximum
329 photosynthesis rate in penultimate leaves and more specifically for carboxylation capacity in
330 flag leaves. Our simulations suggest that diurnal carbon gain is depressed by up to 15% by
331 non-instantaneous induction of photosynthesis in sunflecks, and is up to 4% lower in the
332 "slowest" genotypes that we studied as compared to the "fastest". This complements recent
333 work (Taylor & Long, 2017) documenting the potential impacts on carbon gain of slow
334 Rubisco induction in sunflecks by demonstrating variation in this important trait in available
335 genetic resources, showing that realistic gains are achievable even using traditional
336 breeding.
337
338 *Variation in induction kinetics*
339 Our preliminary analysis of 58 wheat genotypes suggested wide variation in acclimation
340 kinetics, with genotype median t_{95} varying 2.82-fold overall (2.66-fold among the 37
341 genotypes for which we had at least two measurements), and our laboratory study with
342 balanced replication (n=5) within ten genotypes found 1.6-fold variation in genotype
343 median t_{95} for V_{cmax} induction. Up till now there has been little information about diversity of
344 photosynthetic induction kinetics across wheat genotypes, however Soleh *et al*. (2017)
345 found wide variation across 37 soybean cultivars and noted that this variation was
346 genetically determined (i.e. stable across different leaf positions and phenological stages).
347 As in our study in wheat, differences among soybean genotypes were attributed largely to
348 variation in the rate of Rubisco activation. Additionally, induction kinetics were not
349 correlated with steady-state photosynthetic capacity, and there was little evidence for this
350 in our study (Fig S4). This observation, if held true over a broader range of studies has large
351 ramifications for breeding approaches based upon the magnitude of A_{max}, in particular those
352 focused solely on the flag leaf. Based on evidence presented here, efforts to improve net
353 carbon capture across canopies must also consider the responses of A to short term changes

in the environment as a dynamic acclimation property that is at least partially genetically determined (Murchie et al. 2018).

Acclimation of A_{max} in field-grown penultimate leaves differed markedly from acclimation of V_{cmax} in chamber-grown flag leaves. The former was sigmoidal with time, having a lag phase and longer t_{95} (median 12.62 min), whereas the latter was double-exponential with time, with no lag and shorter t_{95} (median 8.25 min). These differences are not necessarily surprising, given the numerous differences between the two experiments; we initially discovered wide variation in t_{95} for A_{max} in the field experiment, and then designed the V_{cmax} experiment to be comparable to that of Taylor and Long (2017) rather than the A_{max} experiment. We note, however, that the 'rise time' ($t_{75} - t_{25}$, the time required for A_{max} or V_{cmax} to rise through the middle 50% of its dynamic range) was more similar between the two experiments (median 3.26 min for A_{max} vs 2.60 min for V_{cmax}) than was t_{95}, which may suggest that different processes give rise to the lag and rise phases. Future work should test for effects of leaf rank and growth environment under otherwise identical conditions, and should aim to determine whether the lag phase observed in A_{max} induction occurs when leaves are pre-acclimated in low PPFD rather than darkness, as is more realistic for leaves in a natural canopy.

Photosynthetic induction has long been known to involve at least two phases. The initial, fast phase to involve availability of RuBP or other Calvin cycle intermediates and is complete within 1-2 minutes (Pearcy 1990), which is consistent with the median t_{95} that we found for the fast phase of V_{cmax} induction (within-genotype median τ_{fast} = 19.1 sec, which gives t_{95} = 57 sec). The slower phase apparently involves light-dependent activation of Rubisco by Rubisco activase (Rca), with time constants of 4-5 min reported for *Alocasia* and *Spinacia oleracea* (Pearcy 1990) (cf. 2.6 – 5.6 min for τ_{slow} in this study). In low light, sugar phosphates bind to Rubisco active sites, inhibiting carboxylation of RuBP. To restore normal function, Rubisco activase (Rca) uses energy from ATP hydrolysis to actively remove these inhibitors. Rca is sensitive to the chloroplast ADP/ATP ratio and redox status and so mediates Rubisco activation in response to light (Carmo-Silva et al. 2015). The variation in Rubisco activation kinetics found among wheat genotypes in our study could possibly be attributed to differences in (1) the total concentration of Rca, (2) the relative concentrations of the α- and

386 β-Rca isoforms to each other, (3) the binding affinities of Rubisco to inhibitors and of Rca to
387 Rubisco, and (4) the localization of Rca relative to Rubisco. In rice, Rca overexpressing
388 mutants maintain higher Rubisco activation states in the dark and respond more quickly to
389 changes in the light environment than wild type plants (Yamori et al. 2012). *Arabidopsis*
390 mutants expressing only the β-Rca isoform – less sensitive to chloroplast redox status and
391 ADP/ATP ratio than α-Rca – had faster photosynthetic induction rates and exhibited
392 increased growth under fluctuating light compared to plants with both isoforms (Carmo-
393 Silva & Salvucci 2013). As for the binding affinities and co-localization of these two enzymes,
394 much less is known (for a review of current knowledge please see Mueller-Cajar et al. 2014)
395 and future work should seek to address these gaps in knowledge. The recent
396 characterization of the wheat Rca gene structure, as well as advances in genomic, proteomic
397 and transcriptomic techniques, should provide a better understanding of these limitations
398 and allow for a more targeted breeding approach to improve photosynthesis under dynamic
399 light conditions (Carmo-Silva et al. 2015).
400
401 We did not measure deacclimation kinetics, but for modeling we assumed deacclimation
402 kinetics in shadeflecks to be slower than acclimation in sunflecks by a factor of 5/3 (1.67),
403 following Taylor and Long (2017). However, other evidence suggests deacclimation kinetics
404 may be much slower still (e.g., 22-30 min in *Alocasia* and *Spinacia*; Pearcy 1990), which may
405 mitigate the inferred benefits of breeding for faster acclimation, as discussed below.
406
407 *Impact of slow induction on photosynthesis*
408 Consistent with the recent report by Taylor and Long (2017), our modeling found that non-
409 instantaneous acclimation of photosynthesis to fluctuating light can reduce daily carbon
410 gain by up to 15%. The present study extends that conclusion by quantifying the potential
411 impact of varying sunfleck duration, canopy position (which influences the relative
412 proportions of time spent by leaves in sunflecks vs. shadeflecks) and leaf orientation.
413 Specifically, we found that the impact of slow acclimation was greatest for short sunflecks,
414 because when sunflecks are similar to or much longer than the t_{95} for acclimation, leaves
415 will be fully acclimated for most of each sunfleck, and thus losing little potential carbon gain.
416 Leaf orientation had very small effects (Fig S5). The effect of canopy position was also fairly

small in most cases (Fig 6), though projected % carbon losses due to slow acclimation were generally greatest at intermediate canopy depths (cumulative LAI = 0.75 m^2 m^{-2}).

An important exception was for leaves of slow-acclimating genotypes in upper canopy layers (LAI = 0.25 m^2 m^{-2}), which our simulations suggested would experience only half as much daily carbon loss as lower-canopy leaves (LAI = 1.5 m^2 m^{-2}) (7.6 vs 15.9%) for very short sunflecks (< 1 min). In fact, for upper-canopy leaves with very short sunflecks, slow-acclimating genotypes actually had a slight advantage over fast genotypes in our simulations (dashed black line in Fig 6b). This is a consequence of the wider range that we observed (and which we used to drive the simulations) for τ_{fast} (upper and lower deciles = 0.54 and 0.05 min, respectively) vs τ_{slow} (5.6 vs 2.6 min). This meant that the faster and thus greater downregulation in "fast" genotypes during short shadeflecks left them at a lower initial photosynthetic rate at the start of the subsequent sunfleck than "slow" genotypes, which outweighed the benefits of their faster upregulation during sunflecks (Fig 7a). For longer shadeflecks, the reverse was true (Fig 7b). However, we emphasize that this result depends heavily on the assumed kinetics of photosynthetic deacclimation during shadeflecks; as noted earlier, we assumed, following Taylor and Long (2017), that the time constants for deacclimation were 1.67 times greater than for acclimation. Had we instead assumed deacclimation to be 4-6 times slower than acclimation, as suggested by some data (Seeman et al 1988; Woodrow & Mott 1989; Way & Pearcy 2012), it is unlikely that 'slow' acclimating genotypes would have a carbon gain advantage except perhaps in extremely brief sunflecks. This highlights the need for future work to quantify the kinetics of deacclimation.

In very short sunflecks, other factors may dominate dynamics of photosynthesis. For example, buffering of high-frequency (10 – 0.1 Hz) fluctuations in light availability by the 'capacitance' afforded by finite metabolite pools can increase the effective light use efficiency of very high sunfleck PPFDs above 100%, as compared to the average photosynthesis rate when the same PPFD is sustained (Pearcy 1990). Rubisco acclimation and deacclimation are probably not relevant to such short sunflecks, which may dominate canopy light regimes under windy conditions, or for plants with very small leaves.

448 By driving our simulations with observed variation in acclimation kinetics within existing
449 genetic resources for wheat, we were also able to quantify the realistic gains in diurnal
450 carbon capture that should be possible with traditional breeding. We found that the slowest
451 genotypes (modeled using the the highest decile for τ_{slow}) gained up to 4% less carbon, daily,
452 than the fastest (modeled using the lowest decile for τ_{slow}), and that the potential gains
453 were greatest for leaves at intermediate canopy positions (LAI = 0.75 and 1.5 m^2 m^{-2}) and
454 for sunflecks of short to intermediate duration (2-16 min) (Fig 6b). Although these potential
455 gains are not as dramatic as the "headline" numbers of 15-20% based on instantaneous
456 acclimation as the target, they are nevertheless worth pursuing and are sufficiently
457 conservative within genotypes to be a feasible target for breeders. We suggest that
458 continuing work should therefore aim to further quantify variation in this important trait
459 across genotypes of wheat, and to identify target genomic regions to assist breeding efforts.
460 In this capacity, we note that our test of the "single-point" A vs c_i method produced very
461 reliable inference of V_{cmax} during induction (Fig S6), suggesting that induction kinetics can be
462 reliably quantified with as little as one-tenth the time investment per leaf as required for
463 the full dynamic A vs c_i method used in this study.
464
465 **Conclusions**
466 Our study has for the first time identified significant variation in the acclimation time of
467 photosynthesis following dark-to-light transitions across a diverse panel of wheat
468 genotypes, under field and controlled conditions. Slow acclimation of photosynthesis
469 reduced daily carbon assimilation by as much as 16%. These results reinforce the findings of
470 Taylor & Long (2017) in highlighting fast acclimation of photosynthesis, in particular the
471 activation of Rubisco, to fluctuating light as a valuable trait for improvement in wheat
472 breeding programs.
473
474

Supporting Information

File S1:

- Appendix S1. Modeling impact of acclimation kinetics on carbon gain.
- Table S1. List of genotypes.
- Figure S1. Phenological stages at time of measurements.
- Figure S2. Validation of A_{max} in TPU-limited conditions.
- Figure S3. Intercellular [CO_2] at RuBP carboxylation/regeneration transition during induction.
- Figure S4. Relationship between final A_{max} and V_{cmax} rates and t_{95} and $t_{75} - t_{25}$.
- Figure S5. Effect of leaf orientation on diurnal carbon losses due to slow induction.
- Figure S6. Comparison of default and "one-point" A vs. c_i fitting methods.

File S2:

- R script for dynamic A vs ci curve fitting
- R script for analysis of acclimation kinetics

File S3:

- CSV file containing extracted kinetics parameters.

Acknowledgements

This research was supported by the International Wheat Yield Partnership, through a grant provided by the Grains Research and Development Corporation (US00082). TNB was supported by the Australian Research Council (DP150103863 and LP130100183) and the National Science Foundation (Award #1557906). This work was supported by the USDA National Institute of Food and Agriculture, Hatch project 1016439.

References

Bernacchi CJ, Singsaas EL, Pimentel C, Portis ARJ, Long SP. 2001. Improved temperature response functions for models of Rubisco-limited photosynthesis. *Plant, Cell and Environment* **24**, 253-259.

Busch FA, Sage RF, Farquhar GD. 2018. Plants increase CO_2 uptake by assimilating nitrogen via the photorespiratory pathway. *Nature Plants* **4**, 46-54.

Carmo-Silva AE, Salvucci ME. 2013. The regulatory properties of Rubisco activase differ among species and affect photosynthetic induction during light transitions. *Plant Physiology* **161**, 1645-1655.

Carmo-Silva E, Scales JC, Madgwick PJ, Parry MAJ. 2015. Optimizing Rubisco and its regulation for greater resource use efficiency. *Plant Cell and Environment* **38**, 1817-1832.

De Kauwe MG, Lin YS, Wright IJ, Medlyn BE, Crous KY, Ellsworth DS, Maire V, Prentice IC, Atkin OK, Rogers A, Niinemets U, Serbin SP, Meir P, Uddling J, Togashi HF, Tarvainen L, Weerasinghe LK, Evans BJ, Ishida FY, Domingues TF. 2016. A test of the 'one-point method' for estimating maximum carboxylation capacity from field-measured, light-saturated photosynthesis. *New Phytologist* **210**, 1130-1144.

de Pury DGG, Farquhar GD. 1997. Simple scaling of photosynthesis from leaves to canopies without the errors of big-leaf models. *Plant, Cell and Environment* **20**, 537-557.

Duursma RA. 2015. Plantecophys - An R package for analysing and modelling leaf gas exchange data. *Plos One* **10**, 13.

Farquhar GD, Caemmerer SV, Berry JA. 1980. A biochemical-model of photosynthetic CO_2 assimilation in leaves of C-3 species. *Planta* **149**, 78-90.

Kromdijk J, Głowacka K, Leonelli L, Gabilly ST, Iwai M, Niyogi KK, Long SP. 2016. Improving photosynthesis and crop productivity by accelerating recovery from photoprotection. *Science* **354**, 857-861.

Lawson T, Vialet-Chabrand S. 2018. Speedy stomata, photosynthesis and plant water use efficiency. *New Phytologist*.

Long SP, Zhu XG, Naidu SL, Ort DR. 2006. Can improvement in photosynthesis increase crop yields? *Plant Cell and Environment* **29**, 315-330.

Morales A, Kaiser E, Yin X, Harbinson J, Molenaar J, Driever SM, Struik PC. 2018. Dynamic modelling of limitations on improving leaf CO_2 assimilation under fluctuating irradiance. *Plant, cell & environment* **41**, 589-604.

Mueller-Cajar O, Stotz M, Bracher A. 2014. Maintaining photosynthetic CO_2 fixation via protein remodelling: the Rubisco activases. *Photosynthesis Research* **119**, 191-201.

Murchie EH, Kefauver S, Ortega JLA, Muller O, Rascher U, Flood PJ, Lawson T. 2018. Photosynthesis: a fast-changing process in an even faster world (Invited Review). *Annals of botany* **122**, 207-220.

Pearcy RW. 1990. Sunflecks and photosynthesis in plant canopies. *Annual Review of Plant Physiology and Plant Molecular Biology* **41**, 421-453.

Portis AR, Salvucci ME, Ogren WL. 1986. Activation of ribulosebisphosphate carboxylase/oxygenase at physiological CO2 and ribulosebisphosphate concentrations by Rubisco activase. *Plant Physiology* **82**, 967-971.

Retkute R, Townsend AJ, Murchie EH, Jensen OE, Preston SP. 2018. Three-dimensional plant architecture and sunlit–shaded patterns: a stochastic model of light dynamics in canopies. *Annals of botany*.

Salter WT, Gilbert ME, Buckley TN. 2018. A multiplexed gas exchange system for increased throughput of photosynthetic capacity measurements. *Plant Methods* **14**, 80.

Seemann JR, Kirschbaum MUF, Sharkey TD, Pearcy RW. 1988. Regulation of ribulose-1,5-bisphosphate carboxylase activity in *Alocasia-macrorrhiza* in response to step changes in irradiance. *Plant Physiology* **88**, 148-152.

Slattery RA, Walker BJ, Weber AP, Ort DR. 2018. The impacts of fluctuating light on crop performance. *Plant Physiology* **176**, 990-1003.

Soleh MA, Tanaka Y, Kim SY, Huber SC, Sakoda K, Shiraiwa T. 2017. Identification of large variation in the photosynthetic induction response among 37 soybean *Glycine max* (L.) Merr. genotypes that is not correlated with steady-state photosynthetic capacity. *Photosynthesis Research* **131**, 305-315.

Soleh MA, Tanaka Y, Nomoto Y, Iwahashi Y, Nakashima K, Fukuda Y, Long SP, Shiraiwa T. 2016. Factors underlying genotypic differences in the induction of photosynthesis in soybean *Glycine max* (L.) Merr. *Plant Cell and Environment* **39**, 685-693.

Taylor SH, Long SP. 2017. Slow induction of photosynthesis on shade to sun transitions in wheat may cost at least 21% of productivity. *Philosophical Transactions of the Royal Society B-Biological Sciences* **372**, 9.

Way DA, Pearcy RW. 2012. Sunflecks in trees and forests: from photosynthetic physiology to global change biology. *Tree Physiology* **32**, 1066-1081.

Woodrow IE, Mott KA. 1989. Rate limitation of non-steady-state photosynthesis by ribulose-1,5-bisphosphate carboxylase in spinach. *Australian Journal of Plant Physiology* **16**, 487-500.

Yamori W, Masumoto C, Fukayama H, Makino A. 2012. Rubisco activase is a key regulator of non-steady-state photosynthesis at any leaf temperature and, to a lesser extent, of steady-state photosynthesis at high temperature. *Plant Journal* **71**, 871-880.

Figure legends

Figure 1. Representative time-courses of simulated PPFD with alternating sunflecks and shadeflecks (solid lines, left axis) and the fraction of time spent in sunflecks by leaves (dashed lines, right axis), for two canopy positions: cumulative leaf area indices of (a) 0.25 $m^2\ m^{-2}$, and (b) 1.5 $m^2\ m^{-2}$. Simulations assumed a constant sunfleck duration of 16 minutes.

Figure 2. Two examples of dynamic A vs c_i curves, for a leaf with relatively slow acclimation of photosynthesis to light (a; time for V_{cmax} to increase by 95% of the difference from its initial value to its final value, t_{95} = 12.5 min), and a leaf with faster acclimation (b; t_{95} = 5.8 min). In each panel, each curve comprises a Rubisco carboxylation-limited segment (solid lines) and an RuBP regeneration-limited segment (dashed lines), and four curves are shown, each corresponding to a different time after exposure to saturating PPFD (yellow: 1 min; orange: 2.5 min; green: 7.5 min; blue: 15 min).

Figure 3. Representative time-courses of CO_2- and light-saturated net assimilation rate measured in field-grown plants (A_{max}; a) and carboxylation capacity inferred from dynamic A vs c_i curves measured on chamber-grown plants (V_{cmax}; b). The time at which A_{max} or V_{cmax} rose through 95% of its dynamic range (t_{95}) is shown with a vertical grey bar in both panels. Solid black lines indicate model fits (a: Eqn 3; b: Eqn 2); in (b), the dashed and dash-dot lines represent the fast and slow phases of the model for V_{cmax} induction, respectively (each adjusted to the same asymptote as the full model).

Figure 4. Distribution of values of (a,c) t_{95} and (b,d) t_{75} - t_{25}, the time for Amax (a,b) or Vcmax (c,d) to increase through 95% of its dynamic range (t95), or through the middle 50% of its dynamic range (t75 – t25). 58 genotypes were studied for (a) and (b), of which 37 had 2-4 replicates; 10 genotypes were studied for (c) and (d), each with 5 replicates. The center line in each box plot indicates the median, the upper and lower bounds of each box indicate the 75th and 25th percentiles, respectively, the whiskers indicate the 90th and 10th percentiles, respectively, and the black circles indicate individual values above or below the latter percentiles. Distributions for all genotypes combined are shown at right.

Figure 5. Time-courses for acclimation of normalized V_{cmax} for leaves using the lower decile (orange line) and upper decile (blue dashed line) for the time constants, τ_{slow} and τ_{fast}, of the slow and fast phases of V_{cmax} acclimation. Blue line: τ_{slow} = 5.4 min, τ_{fast} = 0.54 min; orange line: τ_{slow} = 2.6 min, τ_{fast} = 0.05 min.

Figure 6. Simulated percent loss of potential total diurnal carbon gain caused by slow acclimation of photosynthesis to fluctuating light. In (a), the baseline for comparison is instantaneous acclimation, and the solid and dashed lines are results using the 10th and 90th percentiles, respectively, of kinetic parameters (τ_{slow} and τ_{fast}, the time constants for the slow and fast phases of acclimation of V_{cmax}) to model acclimation. In (b), the baseline for comparison is the faster-acclimating genotypes represented by solid lines in (a). Black, red, blue and grey lines are simulations at four different canopy depths (0.25, 0.75, 1.5 and 3.0 m^2 m^{-2} cumulative leaf area index, respectively). All results are averaged across a spherical leaf angle distribution using Monte Carlo sampling, as described in the main text.

Figure 7. Simulated dynamics of net assimilation rate during sunflecks, and the acclimated target value of assimilation rate during shadeflecks, showing that fast-acclimating leaves (red symbols) are actually at a disadvantage relative to slow-acclimating leaves (blue symbols) when sunflecks are long and shadeflecks are short, as in panel (a). Simulations are show for horizontal leaves at mid-day at two canopy positions: cumulative leaf area indices of (a) 0.25 m^2 m^{-2} , and (b) 1.5 m^2 m^{-2}. Black symbols are for instantaneous acclimation; red and blue symbols are for "fast" and "slow" acclimation, respectively, which were modeled using the 10th and 90th percentiles, respectively, of parameters for acclimation kinetics (τ_{slow} and τ_{fast}, the time constants for the slow and fast phases, respectively, of acclimation of V_{cmax}). Sunfleck length was the same in all cases (2.0 min), whereas shadefleck length was greater at the lower canopy position to reflect the greater fraction of time spent in shadeflecks by lower-canopy leaves.

Figures

Figure 1

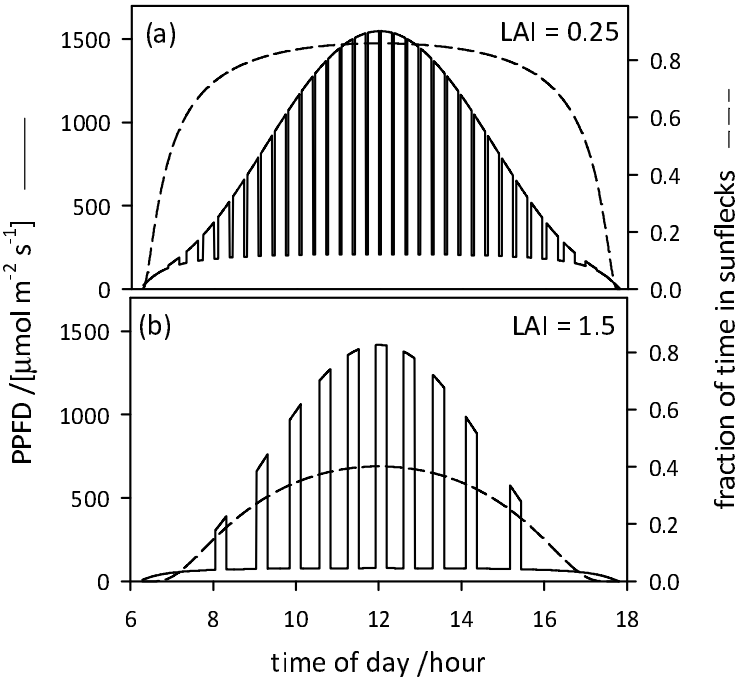

Figure 2

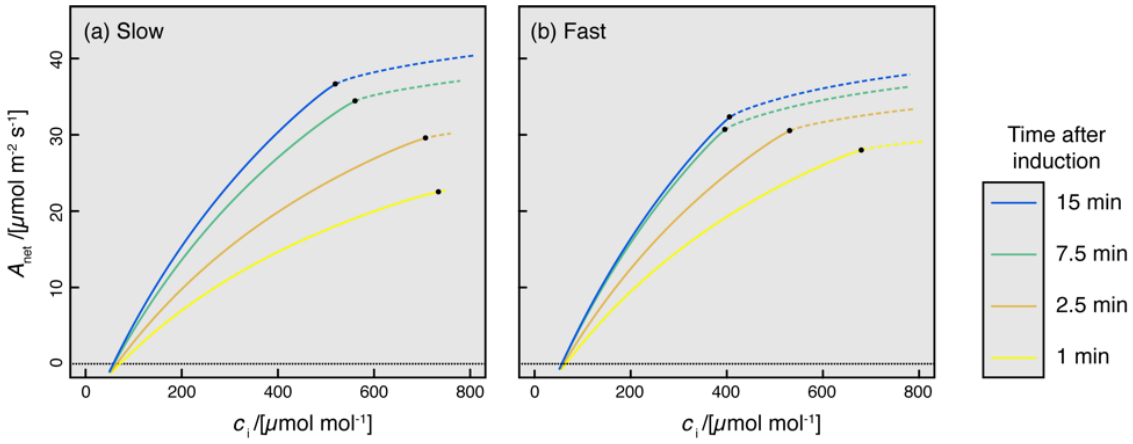

Figure 3

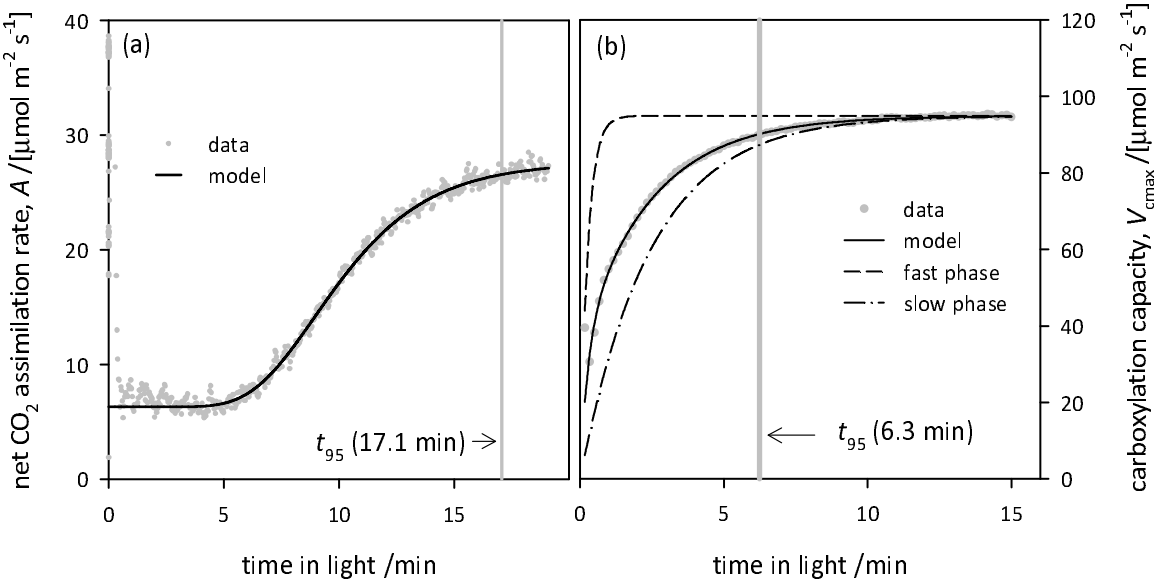

Figure 4

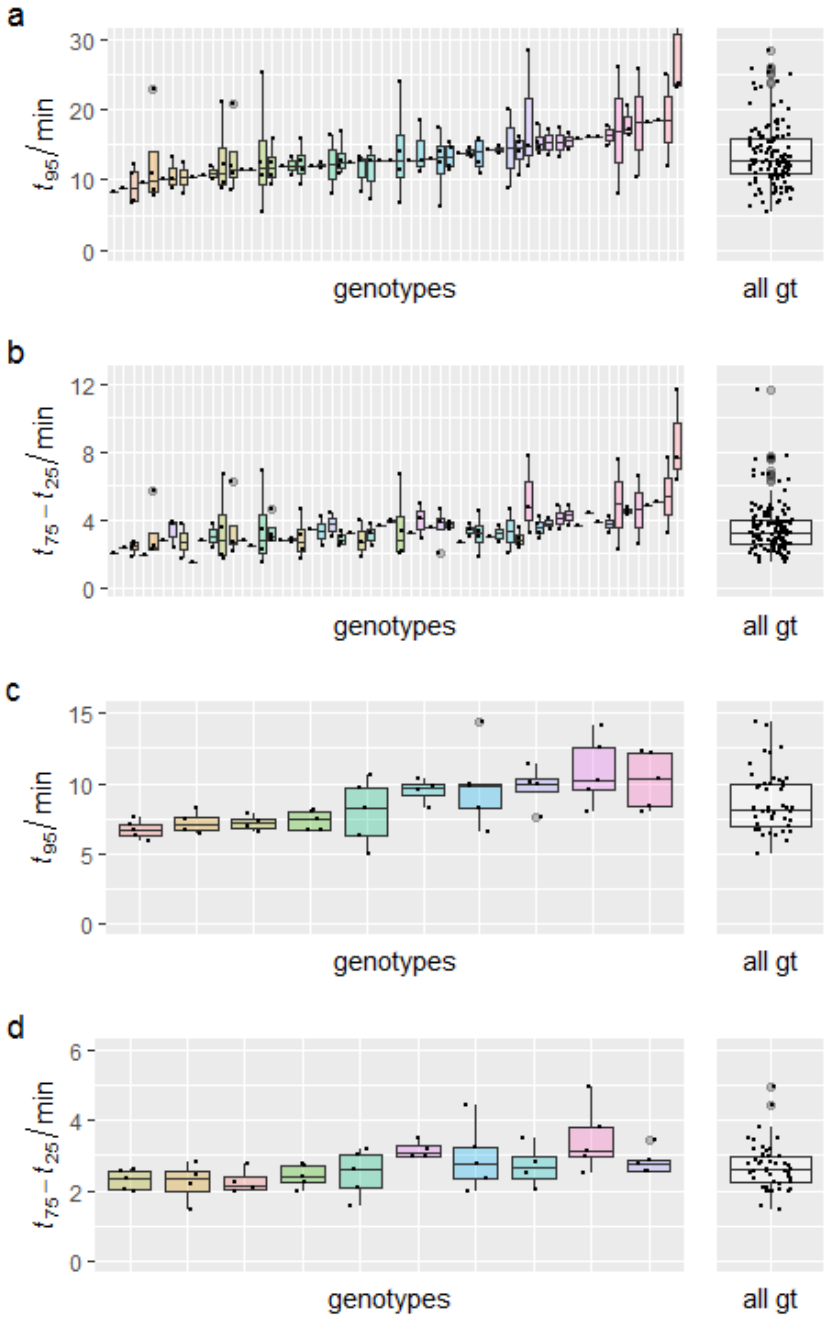

Figure 5

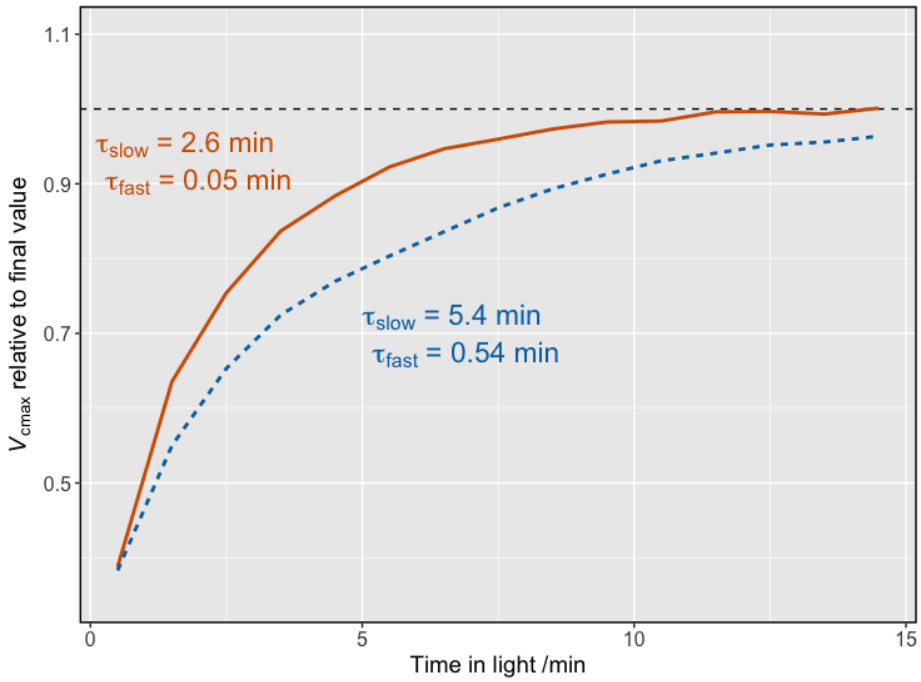

Figure 6

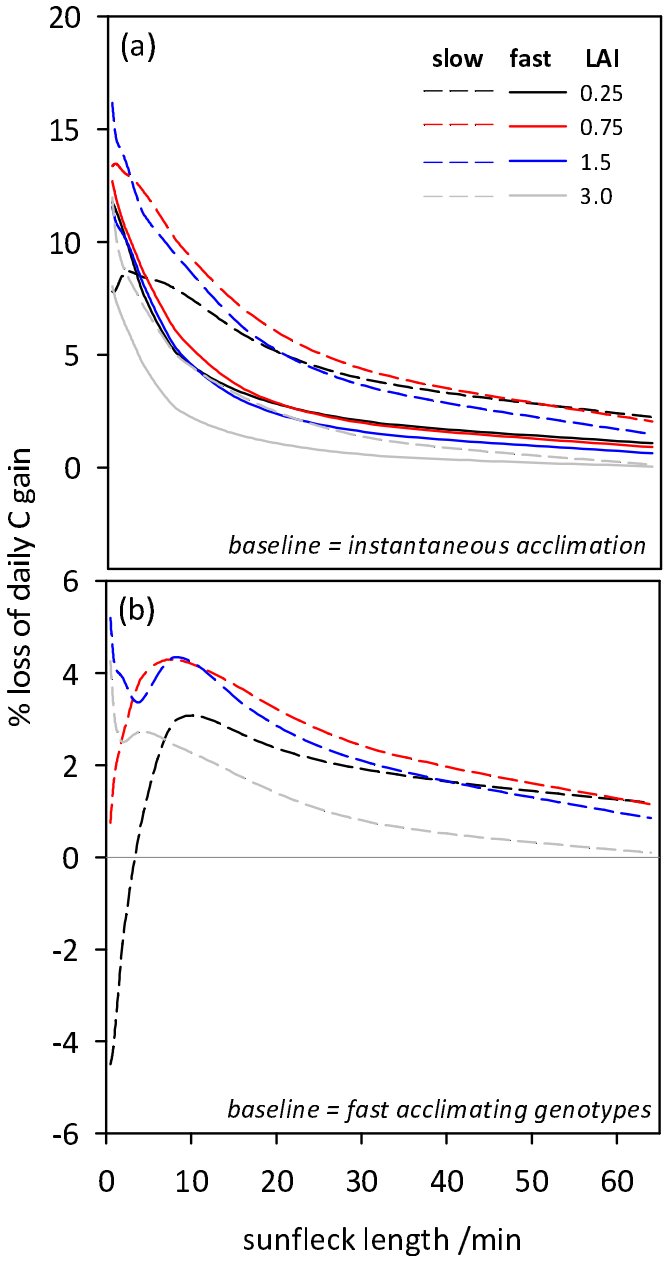

Figure 7